# Size Dependent Properties of Electronic *d*-band of Gold Nano-clusters

**A. Visikovskiy[1], H. Matsumoto[1], K. Mitsuhara[1], T. Nakada[1], T. Akita[2], and Y. Kido[1]**

## Abstract

The electronic *d*-band properties are important factors for the emerging catalytic activity of Au nano-clusters of sub-5-nanometer size. The important *d*-band parameters are d-band width ($W_d$), apparent $5d_{3/2}$-$d_{5/2}$ spin-orbit splitting ($E_{SO}$), and *d*-band center position ($E_d$). We analyzed these *d*-band properties of Au nano-clusters grown on amorphous carbon supports by photoelectron spectroscopy using synchrotron-radiation light coupled with high-resolution ion scattering spectrometry depending on the size of Au nano-clusters. The *d*-band parameters were determined as a function of a number of Au atoms per cluster ($n_A$) and an average coordination number ($n_C$) in a wide range ($11 < n_A < 1600$). The $W_d$ and $E_{SO}$ values decrease steeply with decreasing $n_A$ below ~150 owing to band narrowing which is caused by hybridization of fewer wave-functions of valence electrons. However, $E_d$ shifts to the higher binding energy side with decreasing the cluster size. The rapid movement of $E_d$ is attributed to the dynamic final-state effect, which results in higher binding energy shifts of core and valence states due to a positive hole created after photoelectron emission. Elimination of approximated final-state contribution helps us to estimate initial-state parameters changes depending on cluster size. Modified data still show slight movement of the *d*-band center away from Fermi-level ($E_F$) although the $E_d$ values for Au nano-clusters are closer to $E_F$ compared to the bulk value. This behavior is ascribed to the contraction of average Au-Au bond length with decreasing the cluster size.

[1] *Department of Physics, Ritsumeikan University, Kusatsu, Shiga, 525-8577 Japan*

[2] *Advanced Industrial Science and Technology (AIST) Kansai Center, Ikeda, Osaka 563-8577, Japan*

# I. INTRODUCTION

Gold (Au) is recognized as the most inert metal of the periodic table [1, 2]. It is the only metal which does not form any stable oxides under normal conditions. It is generally accepted that electronic *d*-band structure governs the properties of the noble metals. There is a belief that peculiar combination of the *d*-band propertied such as *d*-band width ($W_d$) and *d*-band position (usually given by the *d*-band center parameter $E_d$) is what makes bulk gold so inert [2]. It is clear, however, that when we considering low-dimensional structures, such as thin layers, nanoparticles or nanorods, the bulk-like configuration of the atoms is compromised and electronic structure may change resulting in change of chemical properties. Two decades ago Haruta *et al.* [3,4] found that the catalytic activity of Au nano-clusters dramatically increases if the cluster size becomes smaller than ~5 nm. Since then, any efforts have been devoted to clarifying the mechanism of the catalytic activity of sub-5-nanometer Au clusters. As the probable factors, the following points have been discussed so far: (i) the effect of metal-insulator transition [5], (ii) charge transfer between the nanoparticle and support [6,7], and (iii) the support mediated strain effect [8]. All of these effects certainly contribute to the catalytic activities of Au nano-clusters; however, it has been shown that the most drastic changes in the catalytic activity can be attributed to changes in the size and shape of Au nanoclusters [9-11]. According to these considerations, the catalytic activity is primarily an intrinsic property of Au nano-clusters. The influence of the support material is mainly indirect, via the shape and size of Au particles [12]. The difference between the bulk inert Au and the active nanoparticles is the relative number of undercoordinated atoms. It has been shown that the dependence of the catalytic activity on the cluster size is well correlated with the average coordination number of Au atoms in the cluster [10]. Nørskov and Hammer proposed so-called "*d*-band model" to explain the trends in the catalytic activities of the metal surfaces, films and clusters [2]. According to this model, adsorbate energy levels interact with metal's *d*-band to produce bonding and anti-bonding states. The position of the *d*-band center influences strength of the interaction and the occupancy of the resulting states, which are directly related to the potential barrier for adsorption as well as the adsorption energy. For bulk Au, the *d*-band lies relatively deep below the Fermi-level ($E_F$) and as a result the antibonding state is thought to be filled, making interaction between the adsorbate and bulk Au repulsive. According to theoretical predictions, with the reduction of the cluster size and increasing the

relative number of undercoordinated atoms, the *d*-band tends to move closer to $E_F$ [9, 13, 14]. Below the certain cluster size the anti-bonding state becomes higher than $E_F$, reducing the potential barriers for adsorption and dissociation. Indeed, the calculations of Phala and van Steen [14] show that the *d*-band center moves approximately 1 eV towards $E_F$ for 1.5 nm Au nano-clusters compared to that of the bulk. The *d*-band theory provides very simple and very general way to predict the properties of the noble metal substances in different state and surroundings. There are, however, some inconsistency between the theoretical predictions and experimental trends observed in some particular cases [15]. Whether the *d*-band theory fails itself or the discrepancies are due to imperfections of theoretical calculations of the *d*-band properties, there is some serious criticism observed among many researchers. Still, it is clear that understanding of the changes occurred in the *d*-band structure with reduction of the cluster size is very important for revealing the origins of the emerging catalytic activity of gold nano-clusters. There are a plenty of theoretical reports on this topic; however, there are a few systematic experimental studies [16-18] on the *d*-band structure of Au nano-clusters.

In the present study, we prepared Au nano-clusters grown on amorphous carbon (a-C) substrates by molecular beam epitaxy and analyzed the properties of the *d*-band by a photoelectron spectroscopy (PES) using a synchrotron-radiation(SR)-light. The average size and shape of the clusters was estimated by a high-resolution medium energy ion scattering spectroscopy (MEIS) and transmission electron microscopy (TEM). We determined *d*-band width ($W_d$) as well as an apparent $5d_{3/2}$- $d_{5/2}$ spin-orbit (SO) splitting ($E_{SO}$), and *d*-band center position ($E_d$) as a function of number of Au atoms per cluster ($n_A$), and average coordination number ($n_C$) in a wide range ($11 < n_A < 1600$).

## II. EXPERIMENTAL DETAILS

We chose a-C as a support for Au nano-clusters for two reasons. First, Au bound weakly to carbon, meaning that interaction with the support does not change the *d*-band structure of Au nano-clusters. Second, a-C gives a relatively weak, smooth and featureless valence band spectrum, which makes it easy to subtract the support contribution from the measured valence band spectra. The a-C layers with thickness of 10 nm were deposited on NaCl(001), KCl(001), LiF(001) and Si(001) substrates by cathodic-arc discharge. We have chosen the alkali-halide substrates to be able to observe Au nano-clusters on a-C by TEM, because the alkali-halide

substrates can be dissolved in water leaving a thin Au/a-C layer on the surface. However, an occasional charge-up effect during photoemission made a spectral analysis to be complicated. In order to suppress the charge-up effect, we deposited Au on the a-C/Si(001) substrates. Note that almost the same a-C layers are grown on alkali-halides and Si(001) substrates, and thus, the size and shape of Au nano-clusters are essentially the same for the all substrates.

Au deposition and all measurements were performed *in situ* at a beam-line 8 named SORIS at Ritsumeikan University SR Center. The beam-line consists of three modules: (i) PES module, (ii) MEIS module, and (iii) a sample preparation chamber. Au nano-clusters have been grown by molecular beam epitaxy (MBE) at deposition rates of 0.1~0.3 ML/min [1 ML=$1.39 \times 10^{15}$ atoms/cm$^2$ corresponding to the areal density of Au(111)].

The size and shape of Au nano-clusters was estimated by high-resolution MEIS using a toroidal electrostatic analyzer employing 120 keV $He^+$ ions. The derailed method for analysis of cluster's size and shape by MEIS was described elsewhere [19]. Basically, for a given type of target atom the mean energy and energy spread of the scattered ions depends on the incident and emerging angles and depth where scattering event has occur (these values are defined as stopping power of the matter and energy struggling). Due to the fact that for the clusters of different shape a depth distribution of the atoms is different, the shape of the MEIS spectra also will be different. By simulating the spectra from different cluster shapes and fitting experimental data we can determine the shape of our gold clusters. The stopping power of Au and $He^+$ fraction were measured in advance for Au thin layers stacked on a slightly oxidized Si(111) substrate. We employed the Lindhard-Scharff formula [20] for energy struggling and an exponentially modified Gaussian line shape in MEIS analysis [21]. After PES and MEIS measurements, the samples were taken to the ambient and transferred to TEM.

Two types of varied space plane gratings in PES equipment cover photon energies from 20 up to 500 eV. We used photons with the energy of 60 and 80 eV for valence band measurements and 140 eV for core-level Au 4*f* spectra. We calibrated the incident photon energy and determined a spectrometer work function using primary and secondary harmonic waves for the Au 4*f* core-levels (assuming binding energy of Au $4f_{7/2}$ to be 84.0 eV) and a Fermi-edge intensity cutoff for the valence band measured on standard polycrystal Au foil. The energy resolution of a hemispherical electrostatic analyzer at the pass energy of 2.9 eV was estimated to be ±0.05 eV.

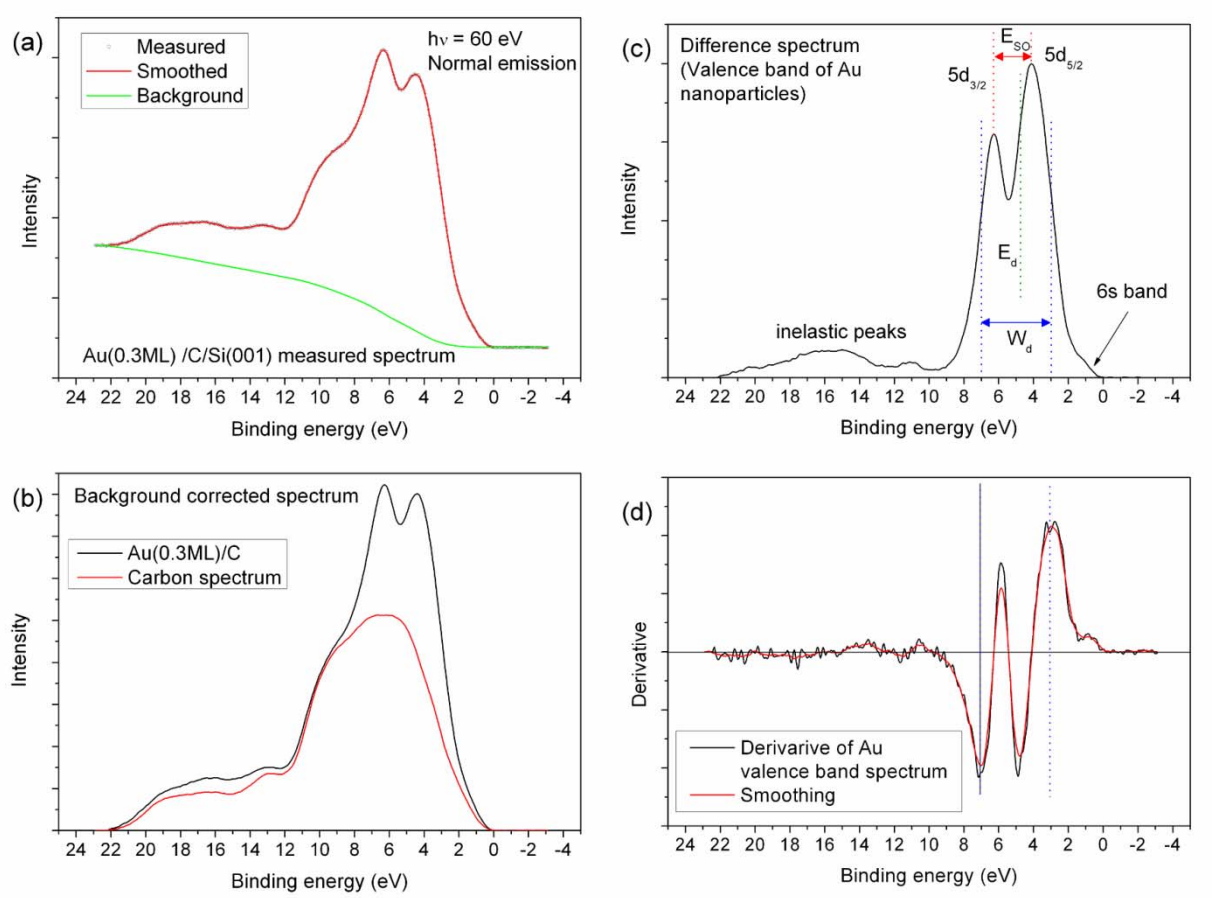


FIG. 1. Au nano-clusters valence band spectra analysis. (a) Measured spectrum of 0.3 ML Au deposited on a-C/Si(001). The spectrum was smoothed and Shirley background was subtracted. (b) Background corrected spectrum of Au(0.3ML)/a-C/Si(001) and a carbon substrate contribution. (c) The ifference spectrum representing Au nano-clusters valence band. The *d*-band parameters $W_d$, $E_{SO}$, and $E_d$ of Au nano-clusters are shown. (d) The derivative of the (c) spectrum and smoothed curve are used to find the points of inflections as boundaries of the *d*-band.

The valence band spectra analysis was performed in a following way. First, the measured spectra, shown in FIG. 1(a) for 0.3 ML Au coverage with black circles, were smoothed, and an inelastic background was subtracted as described in the original work by Shirley [22]. FIG. 1(b) shows the resulting spectrum together with that from a-C which was measured in advance. Each spectrum was normalized by an integrated incident photo-current. The difference spectrum, which is shown in FIG. 1(c), corresponds to the valence band from Au nano-clusters. There are several methods to determine the width of the *d*-band: (i) using FWHM parameters [22, 23], (ii) using on- and off-set points of the *d*-band intensity, and (iii) using points of inflection as boundaries for the *d*-band

[24]. The method (i) is not very reliable as we also have intensity contributions from Au 6*s* band and inelastically scattered electrons. The method (ii) is also difficult to apply, especially at a lower coverage, because of a smooth and continuous transition between the *d*-band intensity and the rest of the spectrum. We adopted the third method as the most reliable because the *d*-band intensity is relatively high and change much faster than the intensity of the *sp*-band or loss peaks, making the position of the points of inflection almost insensitive to the contribution of other parts of the spectra. To find the points of inflection the spectra were differentiated and smoothed aggressively to reduce a noise (see FIG. 1(d)). The apparent Au $5d_{5/2}$-$d_{3/2}$ SO splitting, $E_{SO}$, was determined as a difference in the peaks positions of the Au *d*-band spectra. The *d*-band center, $E_d$, was obtained by calculating a middle point of an integral of the spectra between the inflection points.

We should also comment on concerns about possible angular and photon-energy dependencies of the *d*-band shape in PES spectra. All our PES experiments were performed using the photon energy: 60 (for the alkali-halide substrates) and 80 eV (Si substrates) and 140 eV for Au 4*f* core-level spectra. The energy dependent difference, if any, in the *d*-band parameters measured for all our samples lies within the error limits. We also used the same geometry (normal emission) for all the measurements. Therefore, the possible angular dependence may only come from the orientation of the clusters varied with the size. The Au clusters were grown on amorphous carbon substrates and thus have a random in-plane orientation, although some preferential orientation in a vertical direction cannot be excluded. However, for larger clusters it is unlikely to grow at RT with the preferential orientation varying with the size, and for smaller clusters the *d*-band shape is not very sensitive to the momentum of electrons, as shown in Ref. 16.

## III. RESULTS AND DISSCUSSION

### A. Cluster size and average coordination number

The average size and its dispersion for Au nano-clusters were determined by high-resolution MEIS. FIG. 2(a) shows a typical example of the MEIS spectrum measured for Au(0.05ML)/a-C. It was already demonstrated that the shape of Au nano-clusters on oxides and sputtered HOPG (highly-oriented pyrolytic graphite) substrates is well approximated by a partial sphere with average diameter *d*, height *h*, and size dispersion σ [19]. The best-fit spectrum was obtained assuming a bimodal size distribution of Au clusters, which includes a smaller size group

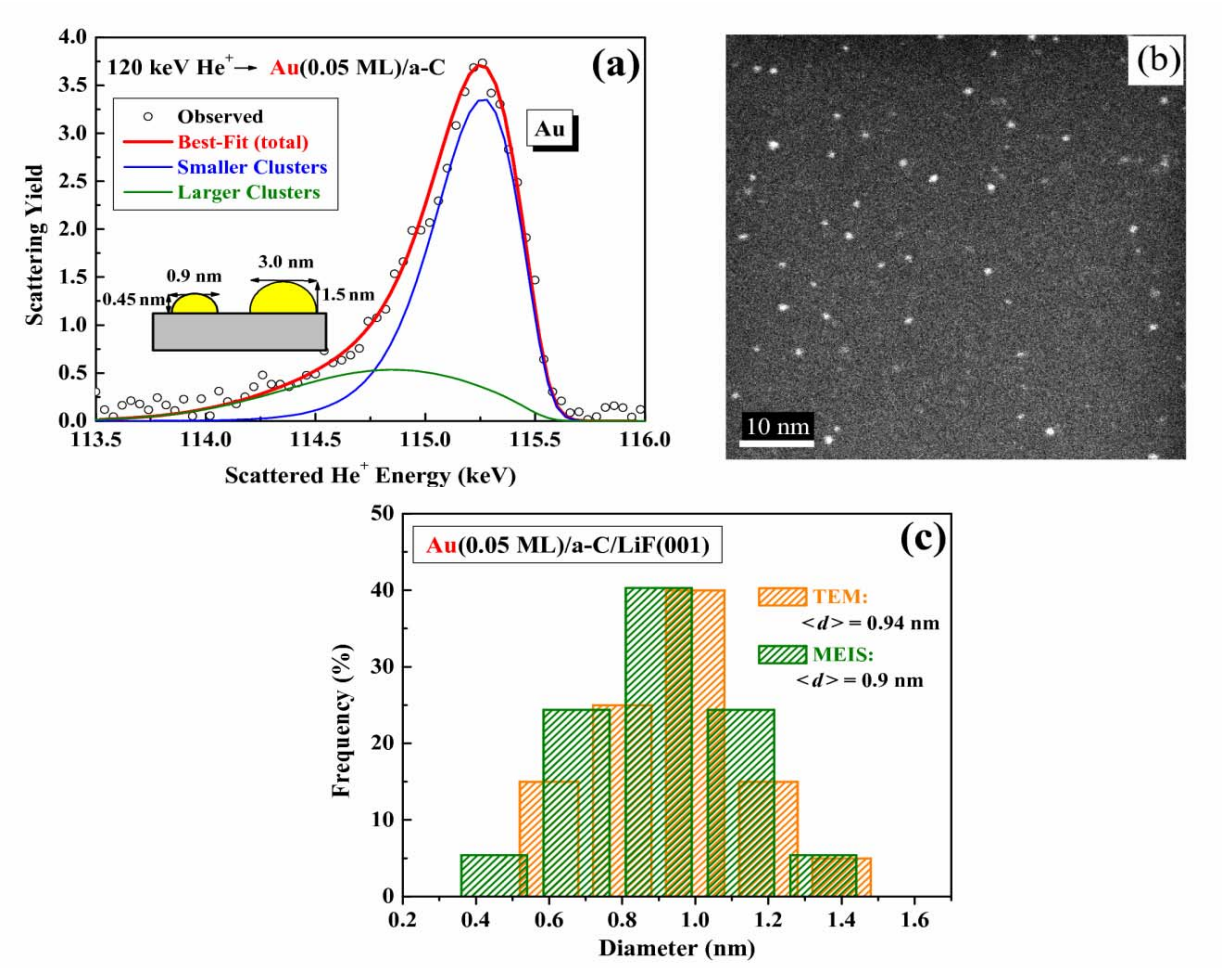


(a) MEIS spectrum observed for 120 keV $He^+$ ions incident on Au(0.05ML)/a-C/NaCl. Incident and detection angles are -45° and +45° with respect to the surface normal. The best-fit (red curve) was obtained assuming a bimodal size distribution with $G_S$ group: $d$ = 0.9 nm, $h$ = 0.45 nm, $\sigma$ = 25 %; and $G_L$: $d$ = 3.0 nm, $h$ = 1.5 nm, σ = 25 %. Volume and areal occupation ratios ($G_L/G_S$) are 0.3 and 0.09, respectively. (b) TEM image for Au(0.05ML)/a-C. (c) A histogram of diameter distributions obtained by MEIS (green) and TEM (orange).

$G_S$ ($d$ = 0.9 nm, $h$ = 0.45 nm, σ = 25%), and a larger group $G_L$ ($d$ = 3.0 nm, $h$ = 1.5 nm, σ = 25%, and a volume ratio, $G_L/G_S$, of ~0.3. This means that the size distribution is asymmetric and for example, an asymmetric Gaussian/Lorentzian profile may also give a good fit. It is, however much simpler to use two symmetric distributions for further analysis, considering the fact that one contribution can be omitted because of the negligible influence on the photoemission spectra. This can be done because $G_L/G_S$ volume ratio of ~ 0.3 corresponds to the areal occupation ratio of

0.09. In PES measurements the kinetic energies of photoelectrons were 30~60 eV, which corresponds to a mean escape depth of ~0.5 nm. Due to this fact, the PES signal ratio from $G_L/G_S$ should be close to the areal occupation ratio, i.e. 0.09; thus, we neglect the contribution from $G_L$ in our analysis. We have also observed the Au cluster size distribution by TEM using the 300 keV electron beam to confirm our MEIS results [FIG. 2(b)]. The size distribution of $d$ (unfortunately present TEM was unable to analyze the height of the clusters) determined by MEIS agrees with that observed by TEM as shown in FIG. 2(c) (only the size distribution of $G_S$ is indicated, as $G_L$ group was omitted). The Au cluster sizes in a wide range of Au coverage are given in TABLE I.

The average number of atoms in each cluster ($n_A$) was calculated assuming a bulk atomic density of Au ($5.90 \times 10^{22}$ atoms/cm$^3$). Calculation of the average coordination number ($n_C$) is a non-trivial task, as it requires knowledge of the exact shape of the clusters. Recently, Pirkkalainen and Serimaa [25] proposed a simple formula to calculate the average coordination number for crystals of a spherical shape depending on their radius,

$$C_{ave} = (1 - y)C_{\infty} + yC_{surf} \qquad (1)$$

where $y = 3t/r$, $C_{ave}$ is the average coordination number of atoms in a nano-cluster, $C_{\infty}$ – the coordination number in a perfect bulk, $r$ is the radius of the particle in unit-cell dimensions, $C_{surf}$ – the average coordination number of surface atoms, and $t$ is a thickness of the surface layer in unit-cell dimensions (for the f.c.c. lattice $C_{\infty} = 12$, $C_{surf} = 7.1606$, and $t = 0.4301$) [25]. The formula is valid for spherical and hemispherical large clusters with a good precision; however, accuracy drops with decreasing the size of the clusters due to shape deviations from the sphere (actual small crystalline clusters have a polyhedral shape). Nevertheless, the extended X-ray adsorption fine structure (EXAFS) measurements [26] and density functional theory (DFT) calculations [27] for the average coordination numbers for small particles agree approximately with the values given by Eq. 1. The size distribution ($\sigma \approx$ 25 %) of Au nano-clusters in our experiment will smooth out a discrepancy between the calculated and actual average coordination number even more. The $n_C$ values calculated using Eq. 1 for Au nano-clusters are also given in TABLE I.

TABLE I. The size of Au nano-clusters determined by MEIS, the average number of Au atoms per cluster ($n_A$) calculated assuming a bulk Au number density, and the average Au coordination numbers ($n_C$) estimated from Eq. 1 proposed by Pirkkalainen and Serimaa [25].

| Au coverage | Diameter $d$±0.1 (nm) | Height $h$±0.1 (nm) | Volume ($nm^3$) | $n_A$ | $n_C$ |
|---|---|---|---|---|---|
| 0.05 ML | 0.9 | 0.45 | 0.19±0.13 | 11.3±7.0 | 6.3±0.6 |
| 0.1 ML | 1.1 | 0.55 | 0.35±0.19 | 20.6±11.2 | 7.3±0.4 |
| 0.2 ML | 1.4 | 0.7 | 0.72±0.30 | 42.4±18.1 | 8.3±0.3 |
| 0.3 ML | 1.8 | 0.75 | 1.15±0.42 | 67.8±25.0 | 9.1±0.2 |
| 0.4 ML | 2.2 | 0.8 | 1.74±0.55 | 103±32 | 9.7±0.1 |
| 0.6 ML | 2.6 | 0.9 | 2.54±0.73 | 150±43 | 10.0±0.1 |
| 0.7 ML | 2.7 | 0.95 | 2.93±0.80 | 173±47 | 10.1±0.1 |
| 0.8 ML | 2.9 | 1.2 | 4.75±1.09 | 280±64 | 10.2±0.1 |
| 1.0 ML | 3.05 | 1.7 | 8.70±1.62 | 513±96 | 10.3±0.05 |
| 1.2 ML | 3.2 | 1.8 | 10.18±1.80 | 600±106 | 10.4±0.05 |
| 1.5 ML | 3.65 | 2.0 | 14.6±2.29 | 859±135 | 10.7±0.03 |
| 2.0 ML | 5.1 | 2.2 | 27.6±3.52 | 1630±207 | 11±0.03 |

### B. Photoemission spectra of the valence band and Au 4*f* core-levels

FIG. 3(a) and 3(b) show the valence and Au 4*f* core-level spectra observed for Au/a-C at different Au coverage. The most obvious feature in the spectra is a shift of the *d*-band and Au 4*f* core-levels to a higher binding energy ($E_B$) side with decreasing the coverage.

The fact of shifting of the spectral features to higher $E_B$ is reflected in FIG. 3(c), where the dependences of *d*-band center and Au $4f_{7/2}$ line positions on cluster size are given. Although, the absolute values of the shift of the *d*-band center and 4*f* core-line differ, their overall behavior is correlated. One may also see that the apparent Fermi-edge onset of the valence band structure in the FIG. 3(a) is smeared and shifted with decreasing the size of the clusters. These features have been observed before for small metallic clusters and often are attributed to transient cluster charging, so-called dynamic final-state effect [37]. Other *d*-band parameters ($W_d$, $E_{SO}$) of the originally measured spectra are shown in FIG. 5(b) and (c).

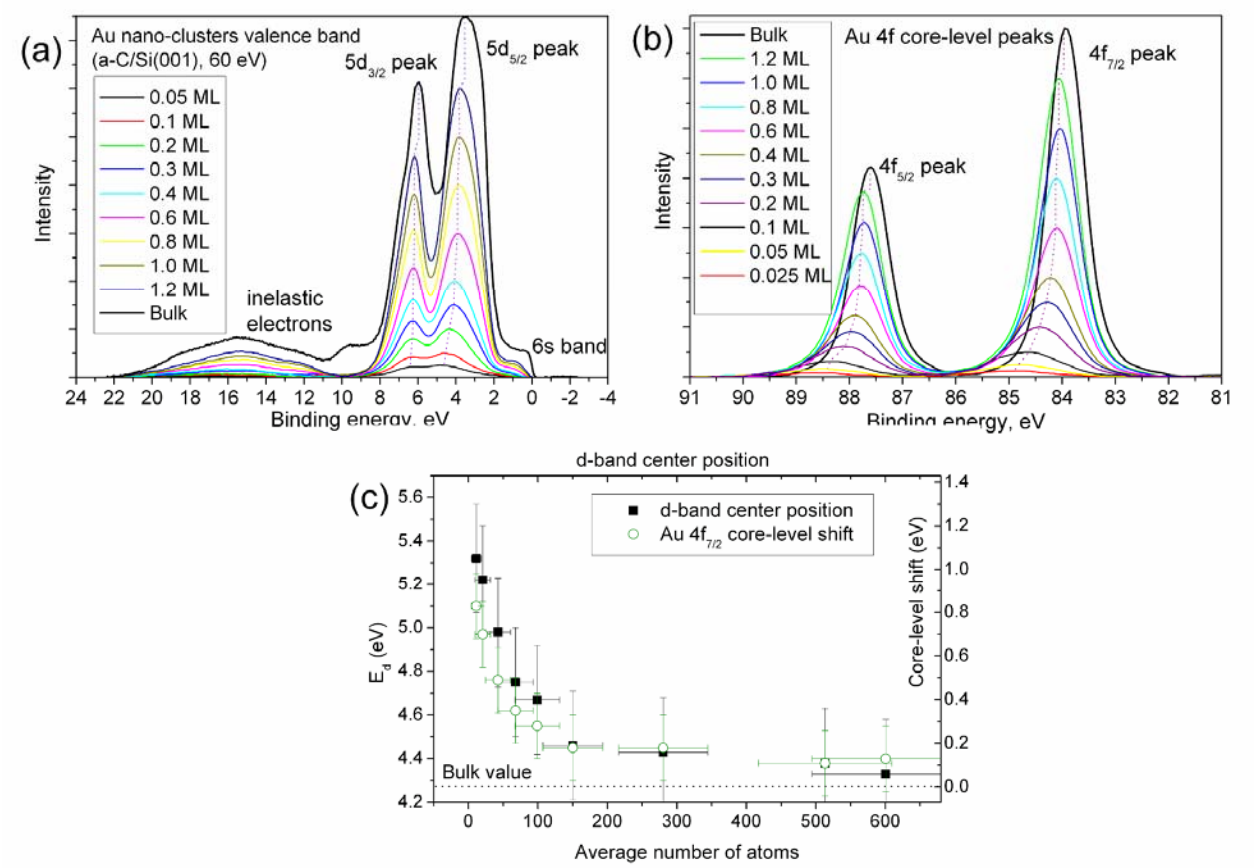


FIG. 3. (a) The valence band spectra of Au nano-clusters (measured at $h\_$ = 60 eV) at different coverage (after a substrate contribution subtraction). The dashed line guides the eye to indicate the shifts of $d3/2$ and $d5=2$ peaks to higher binding energies. The bulk polycrystal Au valence band is also shown for the reference. (b) The Au 4*f* core-level spectra of Au nano-clusters (measured at $h\nu$ = 140 eV) at different coverage. The dashed line guides the eye showing the shift of Au $4f_{5/2}$ and $4f_{7/2}$ lines to the higher binding energies. The bulk polycrystal Au core-level spectrum is also shown for the reference. (c) Derived position of the *d*-band center and shift of the Au $4f_{7/2}$ core-line depending on the cluster size.

The energy of photoelectrons from the valence band as well as core-levels depends on the actual electronic structure of a solid (the initial-state effect) and that is also seriously affected by final-state effects. Our concern is, of course, the dependence of the actual electronic structure of Au nano-clusters on the particle size that is the initial-state effect. Therefore, the final-state effect contribution, which is also dependent on the cluster size, should be removed from the data, if possible, as it is not related to the catalytic properties of Au nanoclusters. The final-state effects are referred to a series of phenomena related to extraction of a photoelectron from an atom that is

relaxation of the electronic structure conduction electrons screening effects and electrostatic Coulomb interaction between the photoelectron and photohole [29-34]. There is still no consensus among the people studying metallic clusters by photoemission technique on what is the main contribution to the observed valence band and core-level peaks shifts. There are some consistent data, however, showing that dependence of relaxation and screening terms of the final-state effect on the cluster size is quite small for weakly interacting substrate such as carbon [35, 36], which was used in our experiments. In the present case, the contribution from the electrostatic Coulomb interaction, so-called the dynamic final-state effect, which comes from electrostatic interaction between an emitted photoelectron and a positively charged cluster, may be very pronounced. This attractive interaction results in higher $E_B$ shifts. The photohole is neutralized within a finite time via tunneling of electrons from the substrate into a metal cluster [37]. The tunneling has a statistical nature with a probability $P(t)dt = (1/\tau)\exp(t/\tau)dt$, where $\tau$ is a relaxation time. Kinetic energy loss, $W$, of the photoelectrons can be expressed by the following probability distribution function,

$$P(W)dW = \frac{C W_{max}}{(W_{max} - W)^2} \exp\left(-\frac{C W}{W_{max} - W}\right) dW \qquad (2)$$

where $C = R/v\tau$, $v$ is a velocity of photoelectron, $W_{max} = \alpha e^2/(4\pi\varepsilon_0 R)$ is a maximum kinetic energy loss, and $\alpha e$ ($\alpha \approx 0.5$ for Au) is an effective charge of the photohole. The equation assumes that Au clusters are spherical with a radius $R$ and the charge is located at the center of the sphere. This distribution results in smearing and shifting of the photoemission spectra even for the clusters of completely identical size. There are several works in which this formalism was used successfully to fit the core-level shifts and the Fermi-edge onset of gold and silver nanoparticles depending on the radius of nanoparticle [38, 39]. In our case the clusters are not spherical, but almost hemispherical, but the mechanism should be the same, it is possible to apply the same expression to our experimental conditions. The only difference is that the $R$ in our case will not correspond to the physical radius of the clusters but to some effective radius reflecting the distance from the surface of the metal cluster to positive image charge of the emitter electron (for normal emission this distance should be close to $h$) So, we also apply this expression to estimate the final-state effect contribution to the *d*-band center shift.

As shown in FIG. 3(a), the apparent Fermi-edge of the valence band spectra moves to the higher binding energy with decreasing of the cluster size. From the shifts of the apparent Fermi-

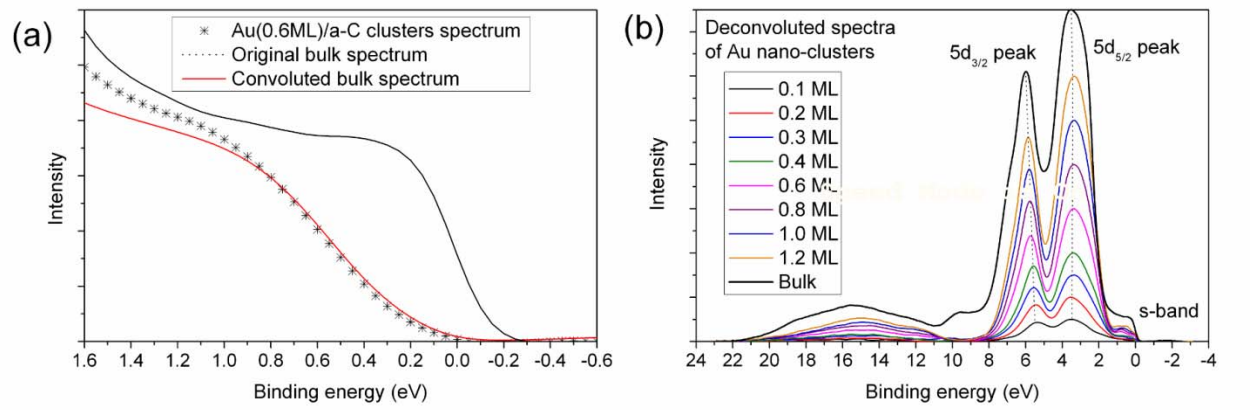


FIG. 4. (a) An example of fitting of the convoluted Fermi-edge spectrum of the bulk Au to the valence band spectrum of Au (0.6 ML) nano-clusters ($\tau$ = 0.5 ps, $R_{ave}$ = 0.85 nm, $\sigma$ = 0.25). (b) Deconvoluted valence band spectra of Au nano-clusters.

edge, its shape, and also from Au 4*f* core-level shifts we may estimate the relaxation time $\tau$ and the effective radius of the clusters. The reference spectrum near $E_F$ and core-level spectrum have been taken from the bulk polycrystal Au foil. These spectra were convoluted using the kinetic energy loss distribution function (Eq. 2) and also accounting for the cluster size distribution as follows,

$$S_{final}(E) = [G(R_{ave}, \sigma) \otimes P(W, \tau, R)] \otimes S_{bulk}(E) \qquad (3)$$

where $S_{bulk}(E)$ and $S_{final}(E)$ are the bulk and convoluted spectra respectively, $P(W, \tau, R)$ is the energy loss distribution for clusters with the radius $R$ (Eq. 2), and $G(R_{ave}, \sigma)$ is a Gaussian size distribution function for the clusters with the average radius $R_{ave}$ and a size dispersion $\sigma$. By best-fitting the convoluted bulk spectra to the observed ones near the Fermi-edge for Au clusters we found that $\tau = 0.50 \pm 0.15$ ps, effective average radiuses $R_{ave} \approx h$, and $\sigma = 0.2 - 0.25$. We must note that $\tau$ is independent of the cluster size because it depends only on a tunneling probability of electrons from the support to the clusters. A typical example of the best fit of the Fermi-edge is shown in FIG. 4(a). Using the same parameters for $\tau$, $R_{ave}$, and $\sigma$ for respective coverage we could also fit well the Au $4f_{7/2}$ core-level spectra (not shown here for brevity); although, some corrections of the peaks positions (0.2-0.3 eV to lower $E_B$) had to be made for

smaller clusters to account the increasing of the surface related component compared to the bulk contribution (the reported $E_B$ difference between the surface and bulk components of Au 4*f* peaks

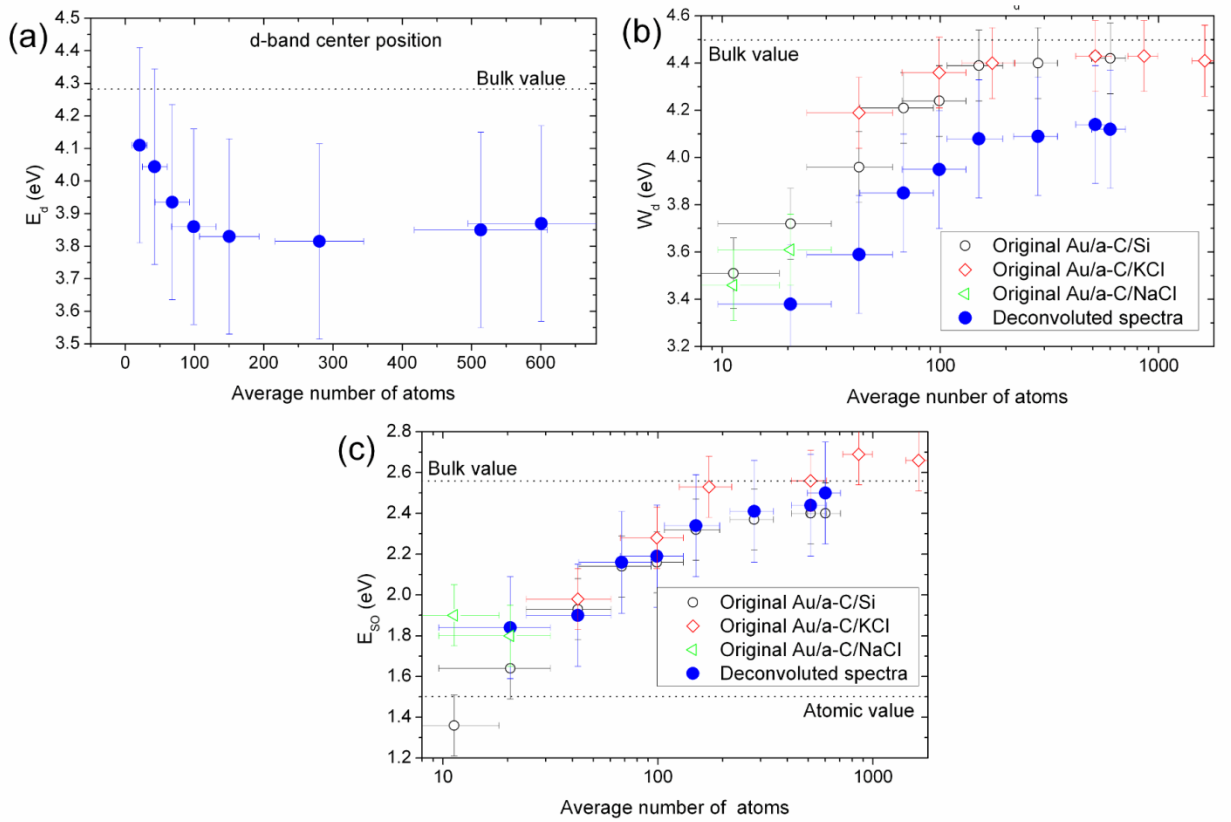


FIG. 5. (a) The *d*-band center derived from the deconvoluted spectra of Au nanoclusters. (b) The comparison between the *d*-band width, $W_d$, measured before (open symbols) and after (filled circles) deconvolution of the spectra. (c) The comparison between the apparent *d*-band spin-orbit splitting $E_{SO}$ measured before (open symbols) and after (filled circles) deconvolution of the spectra. The $n_A$ scale is given in logarithmic scale for the latter two plots to improve data readability.

is 0.2-0.4 eV [40, 41]). After determination of the fitting parameters, the corresponding *d*-band spectrum which reflects the initial-state was obtained by deconvolution using the iterative modified Gold's method [42]. The result is shown in FIG. 4(b). One can see that the Fermi-edge positions of the deconvoluted spectra are now coinciding with the bulk value. Dotted lines in FIG. 4(b) indicate the positions of the *d*-band peaks, $d_{3/2}$ and $d_{5/2}$. The $d_{5/2}$ peak position stays almost constant, while the $d_{3/2}$ peak moves slightly toward lower $E_B$ (~0.45 eV for change in the size from 600 to 20 atoms/cluster).

The *d*-band parameters, $W_d$, $E_{SO}$, and $E_d$, derived from the original and deconvoluted data are given in FIG. 5 as a function of $n_A$. It is clear from the spectra that the parameters of the *d*-band are almost constant for larger clusters and start to change dramatically for $n_A$ below ~150 atoms/cluster. This critical size corresponds to diameter of ~2.6 nm of Au clusters with a shape of partial sphere (close to a hemisphere). The *d*-band width, $W_d$, drops from the value of 4.2- 4.5 eV, which is close to the bulk one, to 3.4 eV with decreasing the cluster size. The apparent $5d_{3/2}$-$d_{5/2}$ SO splitting, $E_{SO}$, is also reduced by ~1 eV from the bulk value of 2.55 eV and reaches approximately the atomic value of 1.52 eV for the smallest clusters with $n_A \approx 11$. The results obtained here for $W_d$ and $E_{SO}$ reflect band narrowing and reducing *d*-orbitals overlap which are caused by hybridization of smaller number of wave-functions of valence electrons for smaller clusters. The apparent SO splitting is a result of an atomic SO splitting and so-called "banding interaction" caused by interaction of the *d*-orbitals of neighboring Au atoms and, thus, depends strongly on the number of nearest neighbors, i.e. the coordination number [24, 28]. Reduction of the apparent SO to almost the atomic value clearly shows significant reduction of the coordination number for smaller clusters. The shift of the *d*-band as a whole is represented by the *d*-band center position as plotted in FIG. 5(a). Although, the shift of the *d*-band is diminished considerably compared with that before deconvolution treatment [see FIG. 3 (c)], still, for cluster sizes below ~150 atoms/cluster, the *d*-band center, $E_d$, moves rapidly to higher $E_B$ values. This result is unexpected, because it contradicts the *d*-band theory predictions [9, 13, 14] and recent theoretical calculations, which stated that the *d*-band moves closer to the Fermi-level with decreasing the cluster size. This is, of course, if we assume a monotonous increasing of the catalytic activity for our particles. At this point we do not have data of activity dependence on size for our clusters, thus we cannot unambiguously conclude on the d-band theory applicability. Interestingly, however, all the *d*-band center positions derived from the deconvoluted spectra for Au nano-clusters take lower $E_B$ values than that for the bulk Au. This means that reduction of a potential barrier for molecular adsorption and dissociation for Au nano-clusters compared to that for the bulk Au may be indeed caused, to some extent, by the *d*-band shifting towards $E_F$. However, the value of the shift is much smaller than predicted one (up to 1 eV according to Ref. 14), and a dependence on the cluster size contradicts a widely accepted theoretical consideration of monotonous movement of the *d*-band center toward $E_F$ with decreasing the cluster size.

One of the possible explanations for contradiction of the observed and expected data is contraction of Au-Au bond in real nano-clusters with size reduction. DFT calculations [27] and EXAFS measurements [43] show that Au-Au bond length is reduced by almost 5% for the clusters with a diameter of ~1 nm compared with bulk Au. This may increase an overlap integral for the *d*-orbitals and push the *d*-band to higher $E_B$ values. In the EXAFS experiments [43] significant reduction of the distance starts when the average coordination number of Au atoms drops below 10. In our experiments this corresponds to the clusters containing ~150 atoms. Indeed, we observe movement of the *d*-band center to higher binding energies staring below ~150 atoms. We have tried to get some supportive information for the above proposal by calculating the *d*-band structure of small Au clusters based on the *ab initio* DFT method using the VASP code [44, 45]. Trial clusters were assumed to take simple cuboctahedral $Au_{19}$, $Au_{38}$ and $Au_{55}$ form (similar to those in Ref. 27). The local density approximation (LDA) approximation has been used because it gives the equilibrium unit cell parameter of 4.06 Å which is in better agreement with the experimental value of 4.08 Å rather than that obtained by the generalized gradient approximation (GGA). Cluster geometries were relaxed until the forces acting on atoms became smaller than 0.01 eV/Å. As a result, all three clusters show inward relaxation of the outermost Au atoms, namely contracting the Au-Au bond from the bulk value of 2.87 Å down to ~2.67 Å depending on location of the outer atoms. The average contraction of the Au-Au bond was ~3% for $Au_{38}$ and $Au_{55}$ and ~4% for $Au_{19}$. All three relaxed clusters show movement of the *d*-band center to higher $E_B$ compared to the unrelaxed geometry. We also performed the calculations in which we manually and uniformly contracted the Au-Au interatomic distance for fixed $Au_{38}$ cluster varying it from 0.98 down to 0.88 of that of the bulk distance with decrement of 0.2. As a result, we obtained a monotonous and almost linear shift of the *d*-band center to higher $E_B$ with decreasing the interatomic distance. Reduction of 4-5% for Au-Au bond length leads to the $E_d$ shift of 0.4 eV away from $E_F$ compared to that for the non-contracted cluster. It is also noteworthy that the present results for $E_d$ dependence on the cluster size are quite consistent with those observed for Au overlayers on Ru(001) substrate [24], where similar shift of $E_d$ to higher $E_B$ has been observed with decreasing Au coverage. As the metallic radius of Au is larger than that of Ru atoms, the first pseudomorphic overlayers of Au experience a compressive stress, which results in contraction of Au-Au distance [lattice mismatch between Au(111) and hexagonal

Ru(001) is 4-5%]. All these facts support our hypothesis of *d*-band movement away from $E_F$ due to the Au-Au bond contraction.

It is important to see other experimental data reported so far to compare with our results. There are several important works studying electronic properties of Au nano-clusters [16, 17].

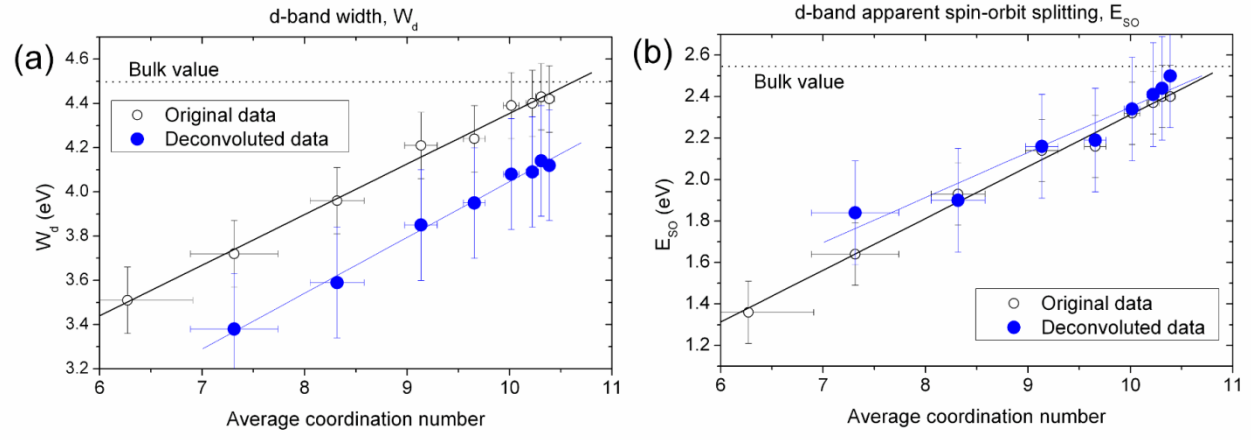


FIG. 6. (a) The *d*-band width ($W_d$) and (b) the apparent *d*-band spin-orbit splitting ($E_{SO}$) depending on the average coordination number of Au atoms in gold nano-clusters. The open circles represent the original measured data; filled circles correspond to the data after deconvolution treatment.

However, apart from our primary interests, these reports only address the *d*-band splitting without the *d*-band center position and the *d*-band width. Actually, our data on $E_{SO}$ agree well with the results obtained in these works. On the other hand, the analysis of the *d*- band, similar to ours, was performed by Bzowski *et al.* [24] for Au thin films on Ru(001). Their results are well consistent with our data obtained here for Au nano-clusters. They found *d*-band narrowing and *d*-band center shifting apart from $E_F$ with decreasing Au coverage. In their study, however, the *d*-band parameters change almost linearly with Au coverage. It is easy to explain this result if we assume that the coordination number of Au atoms plays an important role. The layer-by-layer growth of Au film on Ru(001) means that the number of undercoordinated Au atoms on the surface is almost constant, whereas the number of fully coordinated atoms in inner layers is growing linearly with increasing the coverage. The average Au coordination number should change, therefore, almost linearly resulting in the linear dependence of the *d*-band parameters on Au coverage. In the case of nano-clusters, the average coordination number cannot be expressed by a linear function of the coverage and the cluster size. Indeed, we obtain the linear dependence

of the *d*-band parameters upon the average coordination number of Au atoms calculated using Eq. 1, as indicated in FIG. 6.

We emphasize again that all the *d*-band parameters change dramatically below the critical $n_A$ value of ~150 atoms/cluster. This critical size coincides well with the onset for abrupt reduction of the average coordination number and contraction of Au-Au bond length and also with the onset for emerging catalytic activity of Au nano-clusters reported so far [46, 47].

## IV. CONCLUSIONS

We have studied systematically the *d*-band parameters for Au nano-clusters on a-C in a wide range of cluster sizes ($11 < n_A < 1600$). The cluster size and shape together with the size dispersion were determined by high-resolution MEIS and TEM. Drastic changes take place for all the *d*-band parameters as well as Au 4*f* core-levels for $n_A < 150$ atoms/cluster corresponding to the cluster diameter of ~2.6 nm. The values of the *d*-band width ($W_d$) and the apparent SO splitting ($E_{SO}$) decrease steeply below this critical size. This is a consequence of *d*-band narrowing caused by hybridization of a smaller number of wavefunctions of valence electrons for smaller clusters and of reduction of the coordination number of Au atoms. The *d*-band center shifts apart from the Fermi-level with decreasing the cluster size. This is partly due to the dynamic final-state effect. We tried to derive the initial-state *d*-band spectra of Au nano-clusters by deconvolution treatment assuming a Gaussian clusters size distribution and the formalism of the dynamic final-state effect developed for spherical particles [37]. The deconvoluted data show that the $E_d$ position is closer to the $E_F$ compared to the bulk value; however, it still tends to move away from $E_F$ with decreasing the size of Au nano-clusters. Such a behavior is ascribed to the contraction of average Au-Au bond length with decreasing the cluster size. This trend was evidenced by the *ab initio* calculations. There are some uncertainties included in the deconvolution processing related to both, mathematical procedure itself as well as physical understanding. For example, for the smallest clusters metal-insulator transition may take place and a band-gap may open. This may overestimate the contribution from the dynamic final-state effect. In spite of these difficulties, we believe that present results provide a prominent insight into dramatic changes of the *d*-band parameters of Au nano-clusters and a critical approach to the *d*-band model application. It is also found that the *d*-band parameters such as width and apparent SO splitting are scaled almost linearly with the average coordination number $n_C$, indicating the

importance of the number of undercoordinated atoms in clusters. It is noteworthy that the present data of the *d*-band parameters for Au nano-clusters are quite consistent with those measured for Au overlayers on Ru(001) [24]. The behavior of the *d*-band moving away from $E_F$ observed for thin Au layers and small clusters with decreasing Au coverage and cluster size can be explained by contraction of the Au-Au bond length, suggests the importance of strain upon the *d*-band structures of thin metal films and clusters.

## References


[1] R. Paddephatt, *The Chemistry of Gold* (Elsevier, New York, 1978).

[2] B. Hammer and J. Nørskov, Nature **376**, 238 (1995).

[3] M. Haruta, N. Yamada, T. Kobayashi, and S. Iijima, J. Catal. **115**, 301 (1989).

[4] M. Haruta, Catal. Today **36**, 153 (1997).

[5] M. Valden, X. Lai, and D. Goodman, Science **281**, 1647 (1998).

[6] J.G. Wang and B. Hammer, Phys. Rev. Lett. **97**, 136107 (2006).

[7] A. Sanchez, S. Abbet, U. Heiz, W. Schneider, H. HËakkinen, R. Barnett, and U.Landman, J. Chem. Phys. A **103**, 9573 (1999).

[8] Y. Xu and M. Mavrikakis, J. Phys. Chem. B **107**, 9298 (2003) .

[9] N. Lopez, T. Janssens, B. Clausen, Y. Xu, M. Mavrikakis, T. Bligaard, and J. Nɯrskov, J. Catal. **223**, 232 (2004).

[10] B. Hvolbæk, T. Janssens, B. Clausen, H. Falsig, C. Christensen, and J.K.Nørskov, NanoToday **2**, 14 (2007).

[11] G. Mills, M. Gordon, and H. Metiu, J. Chem. Phys. **118**, 4198 (2003).

[12] T. Janssens, A. Carlsson, A. Puig-Molina, and B. Clausen, J. Catal. **240**, 108 (2006).

[13] T. Jiang, D. Mowbray, S. Dobrin, H. Falsig, B. Hvolbæk, T. Bligaard, and J.K.Nørskov, J. Phys. Chem. C **113**, 10548 (2009).

[14] N. Phala and E. van Steen, Gold Bulletin **40**, 150 (2007).

[15] C. Lu, I. Lee, R. Masel, A. Wieckowski, and C. Rice, J. Phys. Chem. A **106**, 3084 (2002).

[16] S.-T. Lee, G. Apai, M.G. Mason, R. Benbow, and Z. Hurych, Phys. Rev. B **23**, 505 (1981).

[17] H. Kröger, P. Reinke, M. Muttner, and P. Oelhafen, J. Chem. Phys. **123**, 114706 (2005) 18 .

[18] M. Hazama, Y. Kitsudo, T. Nishimura, Y. Hoshino, P. Grande, G. Schiwietz, and Y. Kido, Phys. Rev. B **78**, 193402 (2008)

[19] A. Iwamoto, T. Okazawa, T. Akita, I. Vickridge, and Y. Kido, Nucl. Instrum. Methods B **66**, 965 (2008).

[20] J. Lindhard and M. Scharff, K. Den. Vidensk. Selsk. Mat. Fys. Medd. **27**, 15 (1953).

[21] M. Hazama, Y. Kitsudo, T. Nishimura, Y. Hoshino, P.L. Grande, G. Schiwietz, and Y. Kido, Phys. Rev. B **78**, 193402 (2008).

[22] D. Shirley, Phys. Rev. B **5**, 4709 (1972).

[23] G.K. Wertheim, D.N.E. Buchanan, and V. Lee, Phys. Rev. B **34**, 6869 (1986).

[24] A. Bzowski, T.K. Sham, R.E. Watson, and M. Weinert, Phys. Rev. B **51**, 9979 (1995).

[25] K. Pirkkalainen and R. Serimaa, J. Appl. Cryst. **42**, 442 (2009).

[26] R. Benfield, J. Chem. Soc. Faraday Trans. **88**, 1107 (1992).

[27] O. Haberlen, S. Chung, M. Stener, and N. RËosch, J. Chem. Phys. **106**, 5189 (1997).

[28] G. Crecelius and G. Wertheim, Chem. Phys. Lett. **63**, 519 (1979).

[29] G. Moretti, J. Electron. Spectrosc. **95**, 95 (1998).

[30] S. Kohiki, Appl. Surf. Sci. **25**, 81 (1986).

[31] G. Moretti and P. Porta, Surf. Sci. **287**, 1076 (1993).

[32] R. N. nez Gonzralez, A. Reyes-Serrato, D. Galvran, and A. Posada-Amarillas, Comp. Mater. Sci. **49**, 15 (2010).

[33] M. Yoshiya, I. Tanaka, K. Kaneko, and H. Adachi, J. Phys: Condens. Matter **11**, 3217 (1999) .

[34] G.K. Wertheim and S.B. DiCenzo, Phys. Rev. B **37**, 844 (1988).

[35] D.-Q. Yang and E. Sacher, Appl. Surf. Sci. **195**, 187 (2002).

[36] M.G. Mason, Phys. Rev. B **27**, 748 (1983).

[37] H. HËovel, B. Grimm, M. Pollmann, and B. Reihl, Phys. Rev. Lett. **81**, 4608 (1998).

[38] A. Tanaka, Y. Takeda, T. Nagasawa, H. Sasaki, Y. Kuriyama, S. Suzuki, and S. Sato, Surf. Sci. **281**, 281 (2003).

[39] A. Tanaka, Y. Takeda, I. Imamura, and S. Sato, Appl. Surf. Sci. **237**, 537 (2004).

[40] P. Heimann, J. van der Veen, and D. Eastman, Solid State Comm. **38**, 595 (1981).

[41] A. Tanaka, Y. Takeda, T. Nagasawa, and K. Takahashi, Solid State Comm. **126**, 191 (2003).

[42] P. Jansson, ed., *Deconvolution of Images and Spectra*, 2nd ed. (Academic Press, San Diego, 1997) pp. 114–116.

[43] J. Miller, A. Kropf, Y. Zha, J. Regalbuto, L. Delannoy, C. Louis, E. Bus, and J. van Bokhoven, J. Catal. **240**, 222 (2006).

[44] G. Kresse and J. Furthmuller, Comput. Mater. Sci. **6**, 15 (1996).

[45] G. Kresse and J. Furthmuller, Phys. Rev. B **54**, 11169 (1996).

[46] M. Haruta, Chem. Record **3**, 75 (2003).

[47] T. Fujitani, I. Nakamura, T. Akita, M. Okumura, and M. Haruta, Angew. Chem. Int. Ed. **48**, 9515 (2009).